International Journal of Current Science Research and Review
ISSN: 2581-8341
Volume 08 Issue 01 January 2025
DOI: 10.47191/ijcsrr/V8-i1-36, Impact Factor: 7.943
IJCSRR @ 2025
www.ijcsrr.org

Ultra-High Field Nuclear Magnetic Resonance (NMR) Spectroscopy: Applications at 1 GHz and Beyond

Simon G. Patching
School of Biomedical Sciences (Astbury Building), University of Leeds, Leeds LS2 9JT, UK

ABSTRACT: Nuclear magnetic resonance (NMR) spectroscopy is a powerful non-invasive analytical technique with wide applications that can observe multiple nuclear species at a site-resolved level. Despite this, NMR has inherent low sensitivity compared to other analytical techniques. A principal approach to improve the sensitivity and resolution of the NMR experiment is to increase the strength of the external static magnetic field (B_0), for which the upper practicable limit has gradually increased over five decades. The relatively recent use of high-temperature superconducting materials, such as $Bi_2Sr_2Ca_2Cu_3O_x$ (Bi-2223), $Bi_2Sr_2CaCu_2O_x$ (Bi-2212) or $REBa_2Cu_3O_{7-x}$ (REBCO, RE = rare earth), has enabled construction of ultra-high field NMR magnets. Over twenty commercial ultra-high field NMR instruments at 1.0, 1.1 and 1.2 GHz (23.5, 25.9 and 28.2 Tesla, respectively) have been installed worldwide in the past several years, with more to come. NMR at ultra-high fields benefits both solution-state and solid-state NMR applications. The potential improvements in sensitivity and resolution in NMR spectra are particularly important for studying the structure, dynamics and ligand interactions of biomolecules, which can suffer from poor sensitivity and prohibitive signal crowding. The benefits of using ultra-high field NMR have begun to be demonstrated on various sample types, including intrinsically disordered proteins, membrane proteins, amyloid fibrils, viral capsids, bacterial chlorosomes, fungal cell walls, and whole human cells. Alongside optimisations in sample preparation, probe design and pulse sequences, and exploitation of dynamic nuclear polarisation (DNP), ultra-high field magnets are contributing to an exciting period for improving the sensitivity and resolution of NMR spectra in the study of more complex biomolecules and other samples.

KEYWORDS: Energy levels, Magnetic field, NMR-active nuclei, Resolution, Sensitivity, Signal dispersion, Solid-state NMR, Solution-state NMR.

1. INTRODUCTION

Nuclear magnetic resonance (NMR) spectroscopy is a powerful non-invasive analytical technique with wide applications in the medical, physical and life sciences and in engineering. NMR can be used to analyse the constituents of clinical samples, including the study of small molecules in cells, biological fluids and tissues (metabolomics) (Marchand et al., 2017; Emwas et al., 2019; Horrocks et al., 2022; Weng et al., 2022; Ahmed et al., 2023; Nagana Gowda and Raftery, 2023), and the NMR phenomenon is the basis of the medical diagnostic technique of magnetic resonance imaging (MRI) (Grover et al., 2015; Khashami, 2024). NMR can be used to determine the identities, purities and high-resolution (sub-angstrom) structures of organic and inorganic compounds in solution and in the solid-state and to monitor their reactions (Derome, 1987; Patching et al., 2009; Richards and Hollerton, 2010; Patching, 2017; Quinn et al., 2022; Brown and Su, 2023). NMR is a key technique for studying the structure, function and dynamics of biomolecules, including proteins and nucleic acids (Patching, 2011; Hiruma-Shimizu et al., 2015; Patching, 2015; Yamaoki et al., 2020; Plavec, 2022; Akutsu et al., 2023), and their interactions with other biomolecules and small molecules, including drugs (Kalverda et al., 2014; Emwas et al., 2020; Hu et al., 2022; Caceres-Cortes et al., 2024; Razew et al., 2024). An advantage of NMR over many techniques is that it allows biomolecules to be studied under conditions close to their native environment. NMR can be used to analyse the chemical composition of foods and to monitor changes, important for quality control (Cao et al., 2021; El Sabbagh et al., 2022; Tsiafoulis et al., 2024). NMR can be used to analyse the composition, structure and dynamics of engineering materials, including those for construction (Mauri et al., 2012; Florea et al., 2019; Kruschwitz et al., 2023), carbon capture (Wang et al., 2015; Berge et al., 2022; Pugh and Forse, 2023; Oliveira et al., 2024) and battery fabrication and function (Walder et al., 2021; Shan et al., 2023; Zheng and Greenbaum, 2023; Leifer et al., 2024).

Despite its power for observing multiple nuclear species at a site-resolved level and its wide applications, NMR has an inherent low sensitivity due to the very weak interaction energies that it involves and the limited natural abundance of many NMR-

International Journal of Current Science Research and Review
ISSN: 2581-8341
Volume 08 Issue 01 January 2025
DOI: 10.47191/ijcsrr/V8-i1-36, Impact Factor: 7.943
IJCSRR @ 2025
www.ijcsrr.org

active nuclei (Patching, 2016). Indeed, the sensitivity of NMR is several orders of magnitude poorer than complementary analytical techniques such as mass spectrometry or fluorescence spectroscopy (Lacey et al., 1999). NMR has therefore historically required relatively high sample concentrations (≤ mM) and/or long acquisition times. This review article first considers the reason behind the inherent low sensitivity of NMR, to explain why sensitivity is improved by using stronger external static magnetic fields in the NMR experiment. The development of commercial ultra-high field NMR magnets (≥ 1 GHz) and their current worldwide distribution are then contemplated. Followed by published results of ultra-high field solution-state and solid-state NMR applications on various biological samples.

2. INHERENT LOW SENSITIVITY OF NMR

To understand the inherent low sensitivity of NMR we can look at the basic principles and energy transitions of the NMR experiment (Koutcher and Burt, 1984; Levitt, 2001; Keeler, 2010; Patching, 2016). The isotopes of certain atomic nuclei (those with an odd number of protons and/or neutrons) spin about their axes to generate their own magnetic field, or magnetic moment. These nuclei that possess the property called "spin" behave like tiny bar magnets and are NMR-active. In the absence of a magnetic field, all nuclei are randomly oriented and possess the same energy, but when a magnetic nucleus is placed in an external magnetic field (B_0), it adopts one of a small number of allowed orientations with different energies. The NMR experiment in the simplest case of a spin-1/2 nucleus (e.g. ^{1}H, ^{13}C, ^{15}N) is illustrated in Figure 1. In the magnetic field, the magnetic moments of spin-1/2 nuclei align either with (parallel to, α) or against (antiparallel to, β) to B_0, with a very small excess aligning in the lower energy state. The larger the energy gap (ΔE) between the two states, the larger the difference in their relative populations and the higher the net magnetic polarisation.

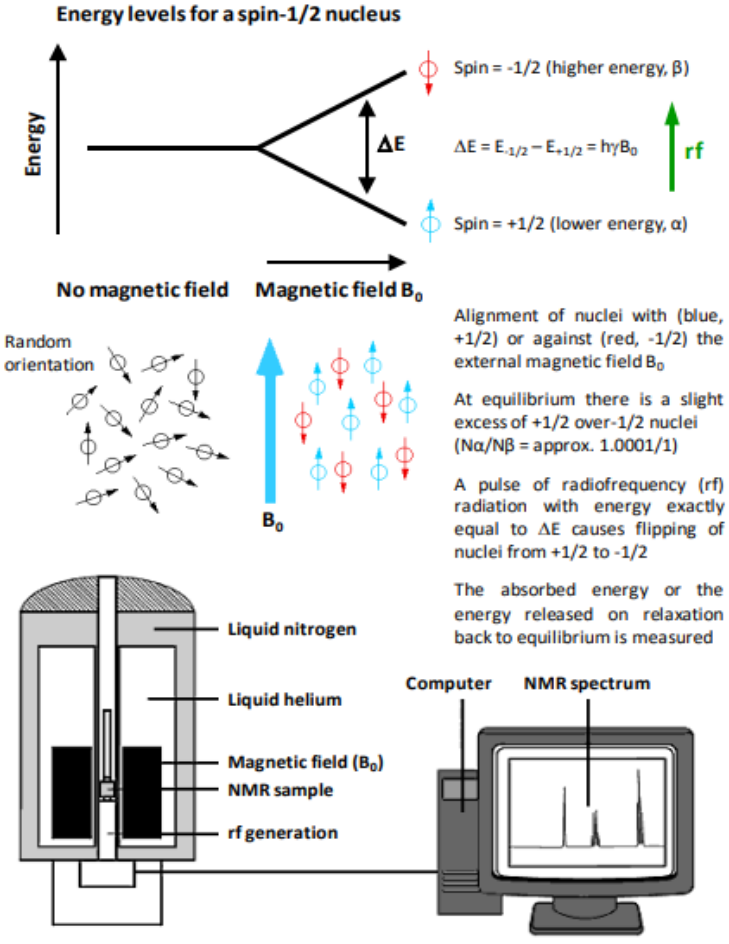

Figure 1. The basic NMR experiment with a spin-1/2 nucleus (e.g. ^{1}H, ^{13}C, ^{15}N). This figure was reproduced from Patching (2016).

International Journal of Current Science Research and Review
ISSN: 2581-8341
Volume 08 Issue 01 January 2025
DOI: 10.47191/ijcsrr/V8-i1-36, Impact Factor: 7.943
IJCSRR @ 2025
www.ijcsrr.org

To produce an NMR signal, radiofrequency (rf) energy is applied at a specific resonant frequency (f_0) to stimulate transitions between the two states as described by equations (1) and (2), where h = Planck's constant (6.62607015 x 10^{-34} J Hz^{-1}) and γ is the gyromagnetic ratio of the observed nucleus.

$$\Delta E = hf_0 \qquad (1)$$
$$f_0 = \gamma B_0/2\pi \qquad (2)$$

This causes nuclei to spin flip from the lower energy state to the higher energy state, and when they relax back to the ground state, rf energy is emitted that can be detected. After thermal equilibrium is reached, the experiment can be repeated. The magnetic field experienced by a specific nucleus in a molecule differs slightly from B_0 such that the exact resonance frequency is dictated by the chemical environment of the nucleus. The main reason for the inherent low sensitivity of NMR compared to other analytical techniques is due to the extremely small population difference between the lower and higher energy states at thermal equilibrium. The Boltzmann distribution law for the population of energy states is described by equation (3), where k is Boltzmann's constant (1.380649 x 10^{-23} J/Kelvin), and T is the temperature in Kelvin.

$$N_{higher}/N_{lower} = e^{-\Delta E/kT} \qquad (3)$$

For example, the population difference between higher and lower energy states for ^{1}H nuclei with a ΔE of 6 x 10^{-24} J at 300 K in a 2.35 T external field is approximately one in 10^5. In other spectroscopy techniques, almost all molecules will begin in their ground state with the excited state essentially at zero.

Different approaches to increase the sensitivity of NMR can be gleaned from a simplified equation (4) for the signal-to-noise ratio (SNR) in an NMR experiment (Webb, 2012; Du, 2023).

$$SNR \propto [\gamma B_0] \times [(\gamma^2 h^2 B_0 N_s)/(16\pi^2 kT)] \times [B_1/I] \times [1/V_{noise}] \qquad (4)$$

The first term relates to the induced voltage, which is proportional to the time rate of change of magnetic flux, and therefore to B_0. The second term is the net magnetic polarisation, where N_s = number of protons in the sample. The third term is the detector sensitivity defined by the magnetic field (B_1) produced per unit input current (I). The fourth term is the random thermal noise voltage with contributions from both the sample and detector (Webb, 2012). In addition to optimising sample preparation strategies, pulse sequences and coils, and exploiting spin-alignment transfer strategies such as dynamic nuclear polarisation (DNP) (Farrar et al., 2000; Barnes et al., 2008; Nawaz and Patching, 2023), one of the principal ways to increase the sensitivity of NMR is to increase the strength of the static magnetic field (B_0) (Ardenkjaer-Larsen et al., 2015). This is because the field strength dictates the Boltzmann population of the nuclear spin levels and their Larmor frequency (Figure 2). The signal increases as the square, and the noise as the square root of B_0, so the SNR increases as $B_0^{3/2}$ (Webb, 2012).

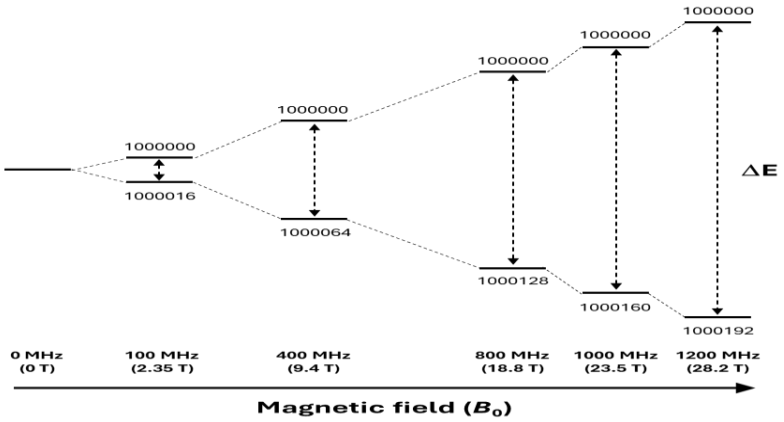

Figure 2. Effect of increasing external magnetic field in a ^{1}H NMR experiment on the relative populations of nuclei in lower and higher energy states at thermal equilibrium, where the population in the higher state is taken as one million.

International Journal of Current Science Research and Review
ISSN: 2581-8341
Volume 08 Issue 01 January 2025
DOI: 10.47191/ijcsrr/V8-i1-36, Impact Factor: 7.943
IJCSRR @ 2025
www.ijcsrr.org

3. ULTRA-HIGH FIELD (≥1 GHz) NMR INSTRUMENTS

The maximum practicable field strength in commercially available NMR spectrometers has gradually increased over the past four to five decades (Moser et al., 2017), reaching ultra-high field at 1 GHz (23.5 T) in 2009 (installed at the Ultra-High Field NMR Center in Lyon, France). Up to this point NMR magnet coils were constructed using low-temperature superconducting (LTS) materials such as NbTi and Nb_3Sn. The use of high-temperature superconducting (HTS) materials, such as $Bi_2Sr_2Ca_2Cu_3O_x$ (Bi-2223), $Bi_2Sr_2CaCu_2O_x$ (Bi-2212) or $REBa_2Cu_3O_{7-x}$ (REBCO, RE = rare earth) (Moser et al., 2017; Park et al., 2020), has enabled the construction of magnets at 1 GHz and above using hybrid design technology with HTS in the inner sections and LTS in the outer sections of the magnet. NMR spectrometers at 1 GHz, 1.1 GHz (25.9 T) and 1.2 GHz (28.2 T) are currently commercially available from the company Bruker (Wikus et al., 2022).

At the time of writing, 1 GHz NMR spectrometers had been installed at the: University of Toronto (Canada), RIKEN (Japan), Weizmann Institute of Science (Israel), University of Barcelona (Spain), University of Birmingham (solution-state) (UK), University of Warwick (solid-state) (UK), Northern Bavarian NMR Centre at University of Bayreuth (Germany). The world's first 1.1 GHz NMR spectrometer was installed in 2019 at St. Jude's Children Research Hospital in Memphis (Tennessee, USA). Further 1.1 GHz spectrometers were installed at the University of Wisconsin's National Magnetic Resonance Facility at Madison (NMRFAM) (USA) (2024) and the University of Georgia Complex Carbohydrate Research Center (USA) (2024). The world's first 1.2 GHz NMR spectrometer was installed in 2020 at the Centro Risonanze Magnetiche (CERM) of the University of Florence (Italy). The world's second 1.2 GHz NMR spectrometer was also installed in 2020 at Eidgenössische Technische Hochschule (ETH) Zürich (Switzerland), and this was the first to be configured for solid-state NMR.

Other 1.2 GHz NMR spectrometers have since being installed at the: Max Planck Institute (MPI) for Biophysical Chemistry in Göttingen (Germany) (2020), uNMR-NL facility, Utrecht University (Netherlands) (2021), Center for Biomolecular Magnetic Resonanc at the Goethe University in Frankfurt (Germany) (2022), Bavarian NMR Center (BNMRZ) in Munich (Germany) (2022), Centre National de la Recherche Scientifique (CNRS), University of Lille (France), Swiss High-field NMR Facility, Zurich site (Switzerland) (2023), Jülich Biomolecular NMR Center (Germany), Leibniz Forschungsinstitut für Molekulare Pharmakologie (FMP) in Berlin (Germany) (2024). The first 1.2 GHz NMR spectrometer in the USA was installed in 2024 at the National Gateway Ultrahigh Field NMR Center at Ohio State University, and the first in the Asia-Pacific region was installed in 2024 at the Korea Basic Science Institute (KBSI). Further 1.2 GHz NMR spectrometers are expected in 2025 at the University of Birmingham (UK) (solution-state) and at the UK High-Field Solid-State NMR Facility, University of Warwick (solid- and solution-state capabilities).

The world's highest field functioning NMR instrument employs a 1.5 GHz (35.2 T) Series Connected Hybrid magnet and is configured for solid-state NMR. This non-commercial instrument, constructed at the National High Magnetic Field Laboratory (Florida State University), became operational in 2016 (Gan et al., 2017).

4. APPLICATIONS OF ULTRA-HIGH FIELD NMR

NMR at ultra-high magnetic fields benefits both solution-state and solid-state NMR applications. The potential improvements in sensitivity and resolution in NMR spectra are especially important for the study of biomolecules, for which the effects of ultra-high fields have begun to be demonstrated in various published works.

4.1. Solution-state NMR applications

A unique application of NMR to biomolecules is its ability to analyse the structure and dynamics of intrinsically disordered proteins (IDPs) and intrinsically disordered regions (IDRs) of proteins at an atomic level (Dyson and wright, 2019; Schiavina et al., 2019; Camacho-Zarco et al., 2022; Schiavina et al., 2022; Shahrajabian and Sun, 2024). The signals in NMR spectra of IDPs and IDRs are often very crowded, so NMR at ultra-high field can significantly improve their resolution to enable a more comprehensive analysis and to widen the applicability to larger and more complex proteins. Schiavina et al. (2024) developed an optimised protocol for ^{13}C-detected solution-state NMR investigation of IDPs at 1.2 GHz. This included demonstrating the effect of ultra-high field on the resolution in 2D CACO spectra of the 140-residue IDP α-synuclein. For example, seventeen out of eighteen glycine residues were resolved at 1.2 GHz that was not possible at the lower magnetic fields of 500 MHz and 700 MHz (Figure 3). At 1.2 GHz it was also possible to resolve most of the resonances from the side chains of aspartate (five out of six Cγ-Cβ), asparagine (three out of three Cγ-Cβ), glutamine (four out of six Cδ-Cγ) and glutamate (thirteen out of eighteen Cδ-Cγ) residues (Schiavina et al., 2024).

International Journal of Current Science Research and Review
ISSN: 2581-8341
Volume 08 Issue 01 January 2025
DOI: 10.47191/ijcsrr/V8-i1-36, Impact Factor: 7.943
IJCSRR @ 2025
www.ijcsrr.org

In-cell NMR can obtain structural and functional information on biological macromolecules in their native cellular environment at atomic resolution (Luchinat et al., 2021a; Gerez et al., 2022; Luchinat and Banci, 2022; Kadavath et al., 2023). But the inherent low sensitivity of NMR limits the applicability of in-cell measurements, which is further limited by the number of molecules of interest in the sample and by the short lifetime of cells in the instrument. Ultra-high field NMR can therefore provide significant benefits to in-cell NMR. Luchinat et al. (2021b) showed the first in-cell NMR spectra recorded at 1.2 GHz on human cells and compared them with spectra obtained at 900 and 950 MHz. Overexpression of α-synuclein and the folded protein carbonic anhydrase (CA II) was carried out in human cells with U-^{15}N labelling and the ^{1}H-^{15}N correlation experiments SOFAST-HMQC and BEST-TROSY were used to compare the sensitivity and resolution of in-cell NMR experiments, respectively (Luchinat et al., 2021b). For α-synuclein there was a clear increase in resolution and sensitivity going from 900 MHz to 1.2 GHz for both whole cells and the lysate. For example, in-cell measurements showed that resolution improved in both dimensions of the SOFAST-HMQC and BEST-TROSY spectra, with the highest increase in resolution in the ^{15}N dimension of the BEST-TROSY spectrum (the linewidth of G86 expressed in ppm decreased by ~31% from 900 MHz to 1.2 GHz) (Figure 4). There were significant increases in sensitivity going from 900 MHz to 1.2 GHz, with improvements of SNR up to ~90% in the SOFAST-HMQC spectra and ~75% in the BEST-TROSY spectra (Figure 5). For CA II, the benefits of a higher magnetic field were less evident (Luchinat et al., 2021b).

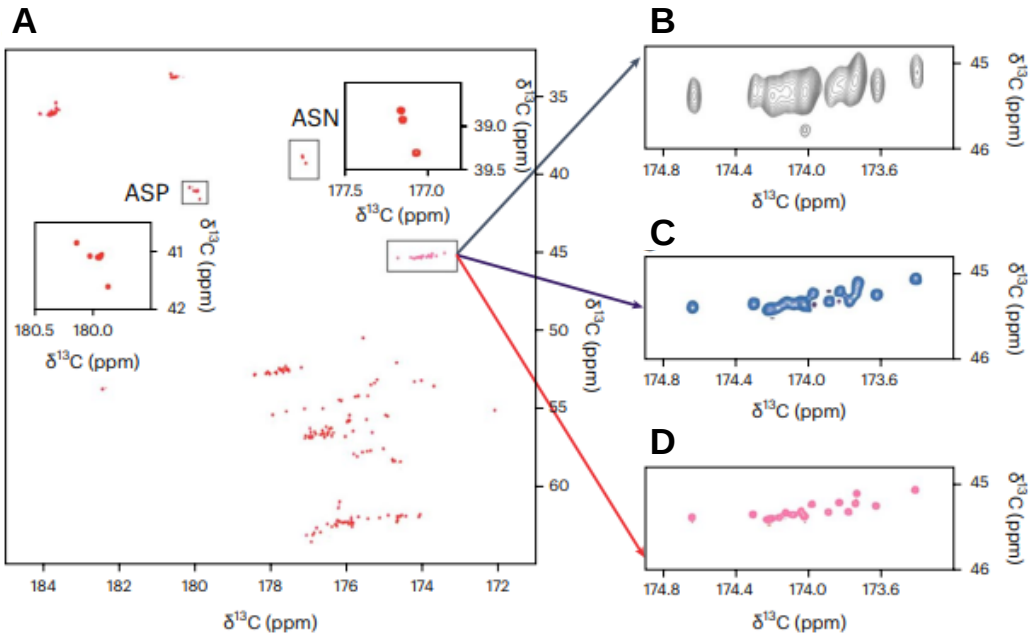

Figure 3. 2D CACO spectra acquired at different magnetic fields. **A.** 2D CACO spectrum acquired using a 1.2 GHz NMR instrument on ^{13}C,^{15}N-labeled α-synuclein (400 µM sample in a solution containing 100 mM NaCl and 20 mM potassium phosphate buffer, pH 7.4). **B-D.** Expansions of the region where the C′-Cα correlation peaks of glycine residues fall, highlighting the increased resolution moving from 500 MHz (grey contours) (**B**) to 700 MHz (light blue contours) (**C**) up to 1.2 GHz (pink contours) (**D**) NMR instruments. This figure was reproduced from Schiavina et al. (2024).

Kaup and Velders (2022) used 1.2 GHz solution-state NMR to investigate the dynamics of polyamidoamine (PAMAM) dendrimer-based micelles. Spectra of the micellar core were obtained with sub-micromolar sensitivity, and diffusion-ordered NMR spectroscopy (DOSY) was used to discriminate released dendrimers from dendrimers still present in the micellar core. The micelles had a hydrodynamic diameter of 40-60 nm based on dynamic light scattering (DLS) and diffusion coefficients measured by NMR predicted a micelle diameter of 43 nm. DOSY NMR showed that the dendrimers residing inside the micelles were rotating fast enough on the NMR time scale to obtain high-resolution spectra.

4.2. Solid-state NMR applications

International Journal of Current Science Research and Review
ISSN: 2581-8341
Volume 08 Issue 01 January 2025
DOI: 10.47191/ijcsrr/V8-i1-36, Impact Factor: 7.943
IJCSRR @ 2025
www.ijcsrr.org

Callon et al. (2021) compared the resolution and sensitivity in ^{1}H- and ^{13}C-detected solid-state NMR spectra of several different biomolecular samples obtained at 850 MHz and 1.2 GHz. The study compared spectra of amyloid fibrils of the fungal prion HET-s(218–289), sediments of the bacterial helicase DnaB, the bacterial RNA helicase and acetyltransferase TmcA, the Rpo4/7 protein complex of two subunits of archaeal RNA polymerase II, the filaments of PYRIN domain of mouse ASC, the viral capsids of the Hepatitis B virus and the African cichlid nackednavirus, supramolecular protein filaments of type 1 pili, and the nonstructural membrane protein 4B (NS4B) of the Hepatitis C virus (Callon et al., 2021). The improvement in spectral resolution was variable but present for all samples. In ^{13}C spectra there were generally substantially higher numbers of peaks were resolved at 1.2 GHz compared to 850 MHz, while for ^{1}H spectra the greatest increase in resolution was achieved for aliphatic side-chain resonances. For example, a comparison of ^{13}C-^{13}C DARR spectra for the DnaB helicase showed a clear improvement in resolution going from 500 MHz to 850 MHz and 1.2 GHz. Indeed, there was an increase from 203 to 322 peaks in the aliphatic region between the 850 and 1.2 GHz spectra (Figure 6) (Callon et al., 2021).

Ultra-high magnetic fields improve the resolution and sensitivity of ^{1}H-detected solid-state NMR spectra obtained with fast MAS. Saurel et al. (2017) used ^{1}H-detected solid-state NMR at 1 GHz with 60 kHz MAS to describe dynamics of the membrane domain of the eight β-strand outer membrane protein A of *Klebsiella pneumoniae* (KpOmpA), which contains four long extracellular loops (L1-L4) and three short periplasmic turns (T1-T3). The transmembrane domain of KpOmpA was reconstituted into proteoliposomes made using *Escherichia coli* polar lipids and NMR measurements were performed on a perdeuterated and amide-reprotonated sample. In the ^{15}N-^{1}H correlation spectrum there was unambiguous assignment of 49 residues (Figure 7). ^{1}H-^{15}N dipolar-coupling and ^{15}N R1 and R1ρ relaxation rates were measured to reveal a collective rocking of the barrel at sub-microsecond timescale and slower residual local motions of residues close to the loops. Proteolysis experiments performed on full length KpOmpA and on its membrane domain, reconstituted in liposomes or in detergent micelles, revealed a unique trypsin cleavage site (in extracellular loop L3) within the membrane domain, which agreed with MAS NMR data (Saurel et al., 2017).

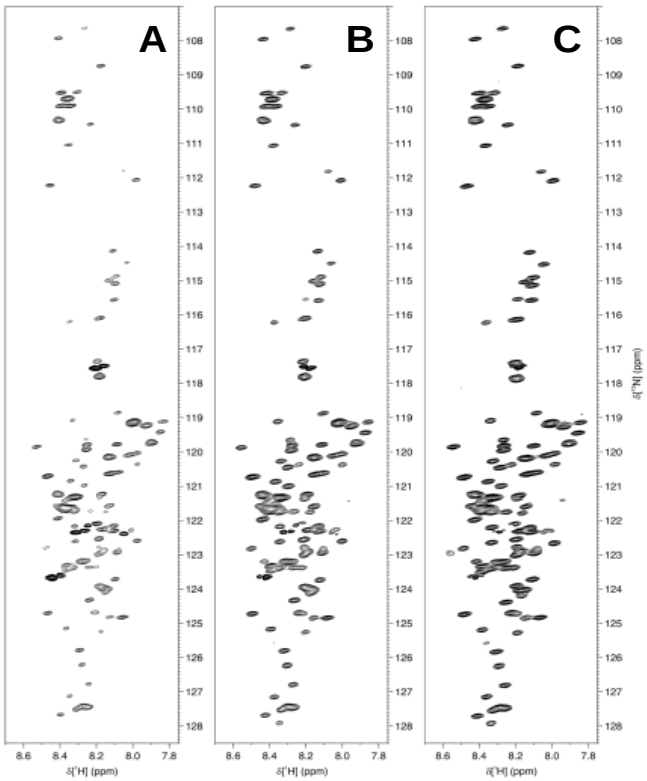

Figure 4. ^{1}H-^{15}N BEST-TROSY spectra recorded at 900 MHz (**A**), 950 MHz (**B**) and 1.2 GHz (**C**) on cells expressing α-synuclein. The spectra were background-subtracted, and the lowest contour level was set to 4x the noise height. This figure was reproduced from Luchinat et al. (2021b).

International Journal of Current Science Research and Review
ISSN: 2581-8341
Volume 08 Issue 01 January 2025
DOI: 10.47191/ijcsrr/V8-i1-36, Impact Factor: 7.943
IJCSRR @ 2025
www.ijcsrr.org

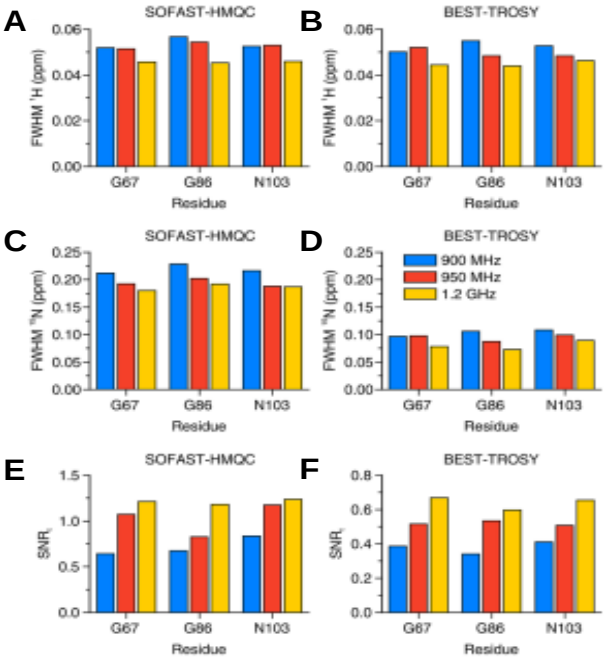

Figure 5. Resolution and sensitivity of α-synuclein in-cell NMR spectra. **A-D.** Spectral resolution of SOFAST-HMQC (**A**, **C**) and BEST-TROSY (**B**, **D**) spectra along the ^{1}H (**A**, **B**) and the ^{15}N (**C**, **D**) dimension, reported as FWHM (ppm) for three peaks at each spectrometer. **E**, **F**. Sensitivity calculated as SNRt = SNR/(t1/2) for each peak in the SOFAST-HMQC (**E**) and in the BEST-TROSY (**F**) spectra. Blue: 900 MHz; red: 950 MHz; yellow: 1.2 GHz. This figure was reproduced from Luchinat et al. (2021b).

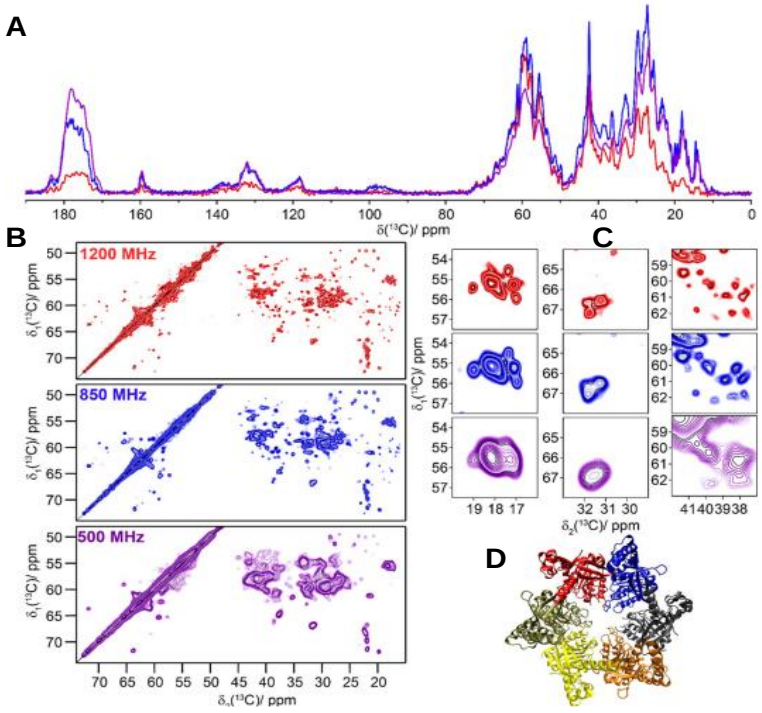

Figure 6. Comparison of ^{13}C spectra at 500, 850 and 1200 MHz for the bacterial DnaB helicase. **A.** 1D ^{13}C-detected CP-MAS spectra recorded at 500, 850, and 1200 MHz. **B.** 20 ms DARR spectra recorded at the same magnetic fields as in A. **C.** Expanded regions from the spectra in B. Spectra coloured in purple were measured at 500 MHz, spectra in blue were recorded at 850 MHz

International Journal of Current Science Research and Review
ISSN: 2581-8341
Volume 08 Issue 01 January 2025
DOI: 10.47191/ijcsrr/V8-i1-36, Impact Factor: 7.943
IJCSRR @ 2025
www.ijcsrr.org

and spectra in red were measured at 1200 MHz. CP was matched at 55 and 29 kHz for ^{1}H and ^{13}C at 1200 MHz and at 60 and 43 kHz at 500 and 850 MHz. The 1D spectra in A were scaled to a similar noise level. **D.** Structural model with each subunit coloured differently (PDB ID: 4ZC0). This figure was reproduced from Callon et al. (2021).

Callon et al. (2023) demonstrated that ultrafast MAS at 160 kHz combined with a 1.2 GHz magnetic field strength significantly improves the resolution of protein side-chain protons in solid-state NMR spectra. Experiments were performed on a model sample, the phosphorylated amino acid *O*-phospho-*L*-serine, and on the hepatitis B viral capsid assembled from 120 core-protein (Cp) dimers. Under these conditions, 61% of the aliphatic protons of Cp could be assigned. NMR spectra of [U-^{13}C, ^{15}N]-labelled Cp149 capsids were acquired using 0.5 mm triple-resonance probe heads and MAS frequencies of 110 and 160 kHz MAS with a sample temperature of ~25 °C. For *O*-phospho-*L*-serine there was a clear decrease in linewidths over the entire range of MAS frequencies (40 to 160 kHz) at magnetic field strengths of both 850 MHz and 1.2 GHz, most prominently for the CH_2 resonances. There were improvements at 1.2 GHz by an expected factor of 1.4 for the H′ and Hg spins (Callon et al., 2023).

For Cp149 there was also a gain in resolution obtained by faster spinning and higher field. In 87 resolved peaks picked from 2D-hCH CP-based spectra (Figure 8) the median total ^{1}H linewidth improved at 1.2 GHz from 207 ± 9 Hz at 110 kHz to 176 ± 7 Hz at 160 kHz MAS. At 850 MHz there was an improvement from 237 ± 14 Hz at 110 kHz to 186 ± 8 Hz at 160 kHz MAS. Hence the move to a higher magnetic field at a constant MAS frequency of 160 kHz also improved the spectral resolution from 186 ± 8 Hz at 850 MHz to 176 ± 7 Hz at 1.2 GHz. Using a combination of MAS at 160 kHz and ^{1}H magnetic field of 1.2 GHz it was possible to assign 61% of the aliphatic protons of the HBV capsid protein and 67% of aliphatic protons having a directly bonded carbon assigned (Callon et al., 2023).

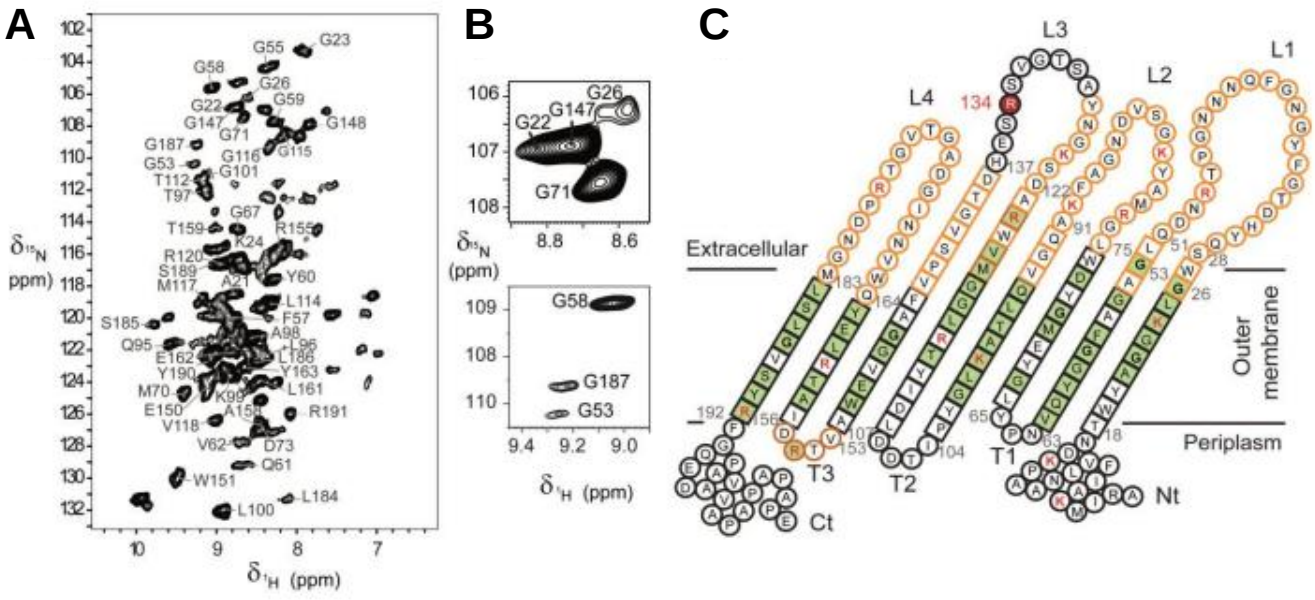

Figure 7. **A.** ^{15}N-^{1}H correlation spectrum of [U-^{1}HN, ^{2}H, ^{13}C, ^{15}N]-labelled N-KpOmpA reconstituted in *E. coli* polar extract liposomes, recorded on a 1 GHz spectrometer and using 60 kHz MAS at 15 °C. Assigned residues are annotated. **B.** Two regions of A containing glycine resonances. Glycine residues at the strand-to-loop transition (i.e. G26 and G53) are weaker compared to G22 and G58 in the same strand and G71 in β-strand 3. C. Topological representation of assigned residues in N-KpOmpA illustrating residue-specific mobility within distinct protein segments and Arg and Lys potential cleavage sites for Trypsin. Residues within β-sheet and random coil regions are represented by square and circles, respectively. Colour code: assigned residues (green), residues exhibiting intermediate timescale motions (orange), Arg and Lys residues (red), unique cleavage site (i.e. R134) accessible to trypsin (red), surrounding residues within loop 3 (black). This figure was reproduced from Saurel et al. (2017).

International Journal of Current Science Research and Review
ISSN: 2581-8341
Volume 08 Issue 01 January 2025
DOI: 10.47191/ijcsrr/V8-i1-36, Impact Factor: 7.943
IJCSRR @ 2025
www.ijcsrr.org

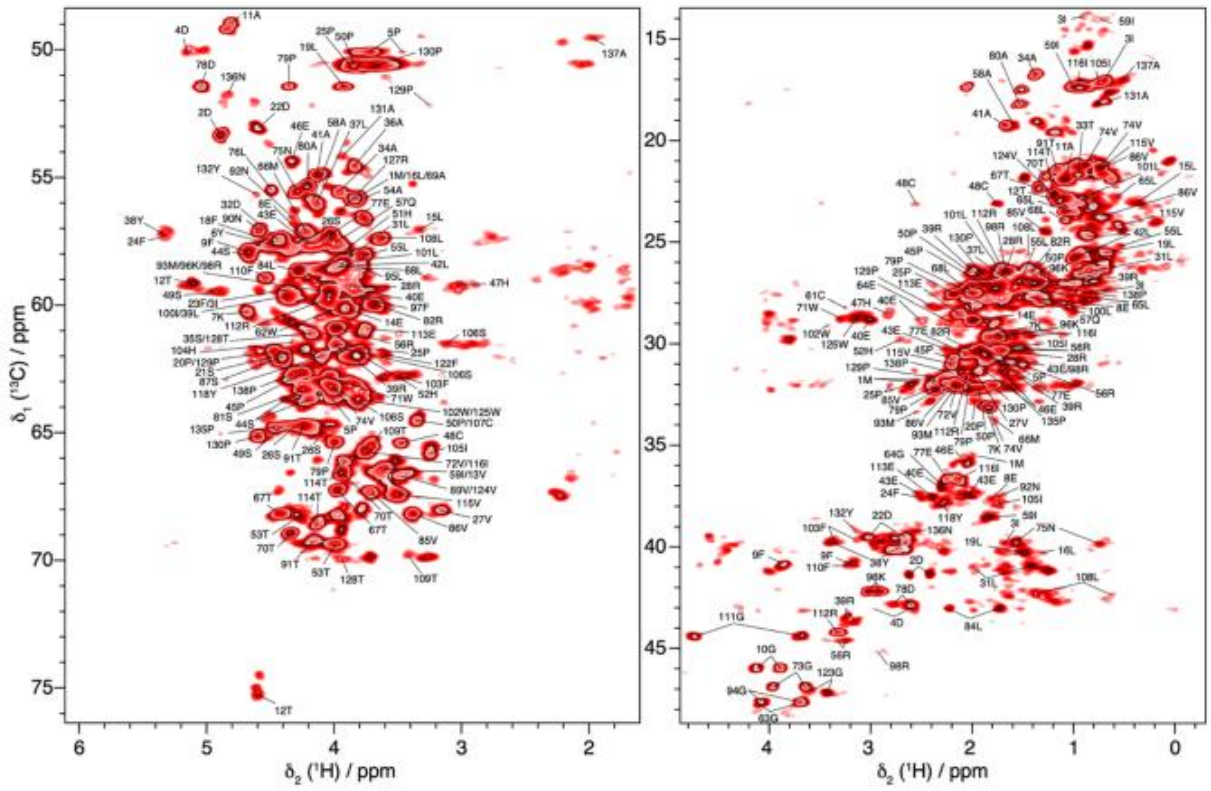

Figure 8. 2D-hCH spectrum of UL-Cp149 measured at 160 kHz MAS frequency and 1200 MHz ^{1}H frequency, with aliphatic ^{1}H assignments obtained from 3D-hNCH and hCCH experiments. This figure was reproduced from Callon et al. (2023).

Schubeis et al. (2020) performed solid-state NMR measurements at 800 MHz and 1 GHz on an eight-stranded β-barrel protein AlkL from *Pseudomonas putida* GPoI that functions as a passive importer of hydrophobic molecules. The sample constituted uniform [^{13}C, ^{15}N]-labelled AlkL (residues 28-230) expressed with a short C-terminal linker and a His_8-tag (total 219 residues) that was reconstituted in DMPC lipid bilayers. NMR spectra at 1 GHz were recorded using a 0.7 mm triple-resonance (^{1}H, ^{13}C, ^{15}N) probe with MAS at 111 kHz. Backbone assignments were achieved for 172 out of 219 residues, which corresponds to 79% total and more than 90% of the detectable residues (Schubeis et al., 2020).

Nimerovsky et al. (2021) compared 2D ^{1}H-detected MAS solid-state NMR spectra of four membrane proteins at 950 MHz and 1.2 GHz. Two helical proteins, the matrix protein 2 (M2) from influenza A, and a citrate sensor (CitA) from *Geobacillus thermodenitrificans*, and two beta-barrel proteins, the human voltage dependent anionic channel (hVDAC) and opacity associated protein 60 (Opa60) from *Neisseria gonorrhoeae*, were studied. In each case, a single fully protonated sample was packed in a 0.7 mm rotor and spectra were recorded at 100 kHz MAS with a sample temperature of around 288 K. There was a consistent improvement in resolution scaling superlinearly with the increase in magnetic field for three of the proteins. In 3D and 4D spectra the resolution improvement resulted in at least 2 and 2.5 times as many signals, respectively. An improvement in sensitivity for the (H)NH and (H)CH spectra of 1.3 ± 0.5 was achieved, consistent with the expected $B_0^{1.5}$ dependence (Nimerovsky et al., 2021).

The conductance domain construct of M2 (residues 18 to 60) with a C50S mutation was expressed with uniform ^{13}C,^{15}N-labelling and reconstituted in DPhPC membranes using d_{78}-phytamoyl, d_9-choline lipids. In a comparison of 2D (H)NH and (H)CH spectra at 950 MHz and 1.2 GHz there was a consistent reduction in the linewidths with an improvement in resolution exceeding the ratio of the magnetic fields (Figure 9). For example, selected amide protons had an improvement factor ranging from 1.23 to 1.55, while the ratio of fields is 1.26 (Nimerovsky et al., 2021).

Uniformly ^{13}C,^{15}N-labelled Gt CitApc (a construct containing the sensor domain [PASp], both transmembrane helices [TM1 and TM2], and the cytosolic PASc domain) with C12A and R93A mutations was reconstituted into a mixture of 1,2-

International Journal of Current Science Research and Review
ISSN: 2581-8341
Volume 08 Issue 01 January 2025
DOI: 10.47191/ijcsrr/V8-i1-36, Impact Factor: 7.943
IJCSRR @ 2025
www.ijcsrr.org

dimyristoyl-*sn*-glycero-3-phosphocholine (DMPC) and 1,2-dimyristoyl-*sn*-glycero-3-phosphatic acid (DMPA) liposomes with a DMPC to DMPA molar ratio of 9:1. The protein to lipid molar ratio was 1:75. Similar to M2, ^{1}H resolution was improved by 20 to 60 Hz at 1.2 GHz compared to 950 MHz, with linewidths of 0.1 to 0.15 ppm (Nimerovsky et al., 2021).

The α-PET hVDAC1 sample was analysed as 2D crystalline preparations in DMPC lipids. Both ^{1}H and heteronuclear linewidths stayed the same in Hz between 950 and 1.2 GHz, resulting in 20% narrower linewidths on the ppm scale (Figure 9) (Nimerovsky et al., 2021).

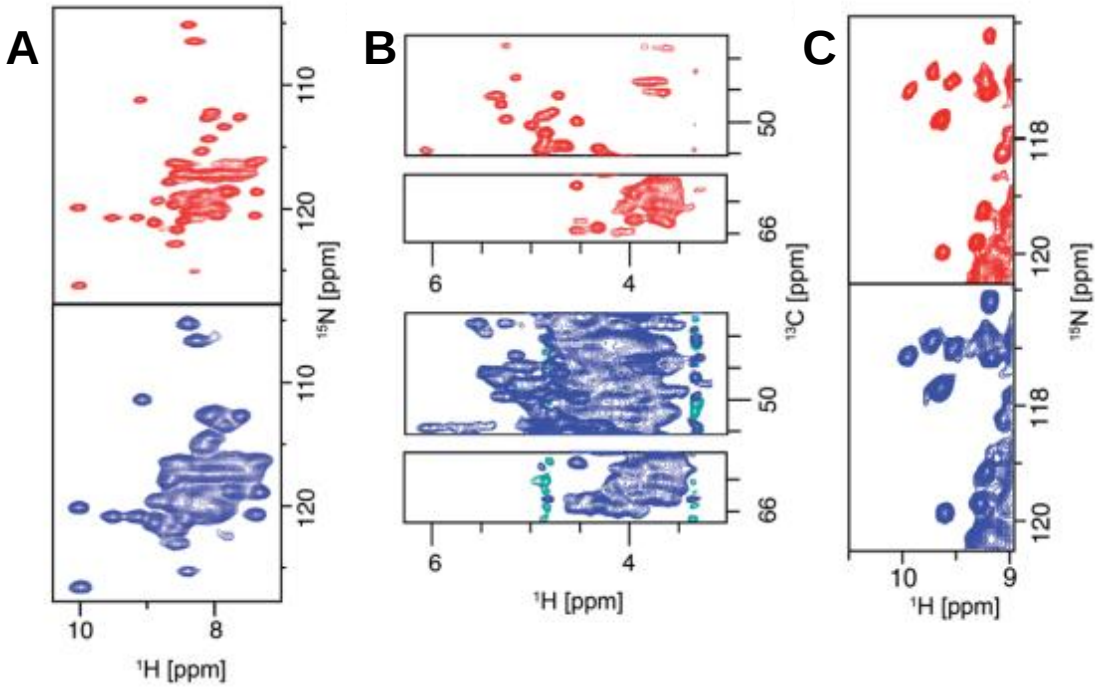

Figure 9. A. (H)NH spectra of fully protonated Influenza A M2 at 950 MHz and 1.2 GHz. **B.** Selections from the alpha region of CP-based HC correlation spectra of CitApc. Spectra were recorded on U-[^{13}C,^{15}N]-labelled CitApc reconstituted in protonated lipids. **C.** (H)NH spectra of crystalline a-PET hVDAC. The MAS frequency was 100 kHz and about 0.5 mg of each sample was used. Measurements at 1.2 GHz = red, 950 MHz = blue. This figure was reproduced from Nimerovsky et al. (2021).

Uniformly ^{13}C,^{15}N-labelled Opa60 was reconstituted into deuterated DMPC lipid bilayers with a lipid-to-protein mass ratio of 0.25. After correcting for the different recycle delays used on the spectrometers, the sensitivity was roughly the same (SNR of 0.9 for (H)NH and 1.0 for (H)CH). But the final CP transfer before detection was shorter for spectra at 1.2 GHz, so the calculations were a lower boundary for sensitivity improvement. ^{1}H linewidths were comparable when measured in Hz but decreased as expected when expressed in ppm (Nimerovsky et al., 2021).

Xue et al. (2019) characterised the interplay between MAS frequency at 70-110 kHz and ^{1}H content on the spectral quality that can be achieved on a 1 GHz spectrometer for methyl resonances. The experiments used microcrystalline samples of the α-spectrin SH3 domain with selectively protonated methyl isotopomers (CH_3, CH_2D, CHD_2) in a perdeuterated matrix. ^{1}H-detected 2D ^{13}C,^{1}H correlation spectra were recorded as a function of MAS frequency at 70-106 kHz, using cross polarization (CP). Two selectively methyl labelled ($^{13}CH_3$, $^{13}CHD_2$) samples of the α-spectrin SH3 domain were used that were otherwise perdeuterated. Spectra for a sample containing $^{13}CH_2D$ isotopomers were estimated by numerical simulations. At 1 GHz it was demonstrated that a MAS frequency above 110 kHz was required to achieve higher sensitivity for all methyl resonances over those labelled at CHD_2. Dinclaux et al. used NMR to explore Ile biosynthesis by monitoring the incorporation of isotope labels, comparing resolution and time requirement at different field strengths ranging from 500 MHz to 1.1 GHz.

International Journal of Current Science Research and Review
ISSN: 2581-8341
Volume 08 Issue 01 January 2025
DOI: 10.47191/ijcsrr/V8-i1-36, Impact Factor: 7.943
IJCSRR @ 2025
www.ijcsrr.org

Chlorosomes are photosynthetic antenna complexes of green sulfur bacteria. Dsouza et al. (2024) performed a structural characterisation of chlorosomes from a bchQ mutant of *Chlorobaculum tepidum* using various biophysical methods, including solid-state NMR at 1.2 GHz with fast MAS at 60 kHz (Figure 10). Nearly complete ^{13}C chemical shift assignments were obtained from well-resolved homonuclear ^{13}C-^{13}C RFDR data. ^{1}H chemical shifts were used to calculate the aggregation shifts, and distance constraints were measured by collecting homonuclear ^{13}C-^{13}C dipolar correlation data. These gave three unambiguous intermolecular correlations (132/31, 132/32 and 121/31) that correlated carbons from ring 1 and ring 3 with distance constraints of less than 5 Å. These constraints indicated a syn-anti parallel stacking motif for the aggregates (Dsouza et al., 2024).

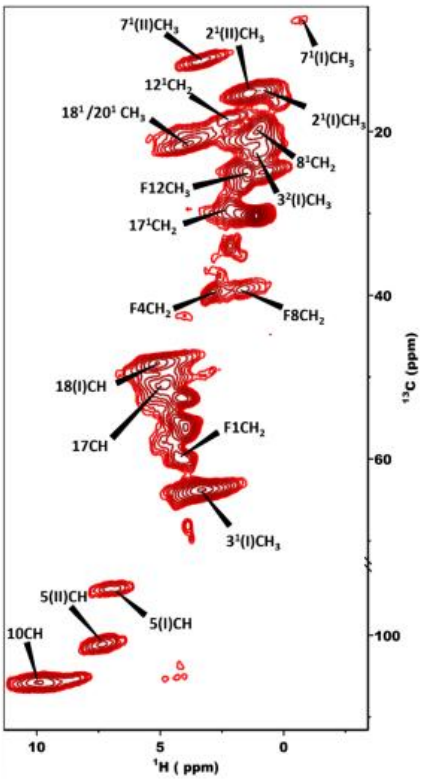

Figure 10. 2D dipolar hCH spectrum of chlorosomes obtained at 1.2 GHz with the sample in a 1.3 mm rotor spinning at 60 kHz at a sample temperature of 277 K. This figure was reproduced from Dsouza et al. (2024).

In a study exploring ^{1}H-detected pulse schemes to probe through-bond ^{13}C-^{13}C networks of mobile protein sidechains, Bahri et al. (2023) used 1.2 GHz MAS NMR to study the cell wall of the fungus *Schizophyllum commune*. hC(c)H spectra with varying TOCSY lengths using WALTZ-16 were compared. The spectra showed multiple bond correlations corresponding to various combinations of C-H pairs within pyranose ring structures and correlations in the amino acid region. The spectra enabled unambiguous assignments for the reducing ends of α and β-glucan (Bahri et al., 2023). 1.2 GHz MAS NMR was used to study various polysaccharides and their location in the dynamic and/or rigid region of the cell wall, and to resolve atom-specific binding events of Cu(II) ions and an antifungal cationic peptide (CATH-2) in the *S. commune* cell wall (Figure 11) (Safeer et al., 2023).

In a structural, chemical, and mechanical characterisation of the fungus *Fomes fomentarius*, Pylkkänen et al. (2023) used MAS NMR at 1.2 GHz to elucidate the composition of major polysaccharides and specific glycosidic linkages in its three different layers, i.e., crust, context and hymenophore tubes. Based on ^{1}H-detected dipolar and scalar ^{1}H-^{13}C correlation experiments it was estimated that the crust layer consisted of 55% of both α-glucan and β-glucan, 1% of chitin, and 44% of other polysaccharides. The context layer consisted of 69% β-glucan, 2% chitin, and 29% of other polysaccharides. Hymenophore tube layers consisted of 38% of β-glucan, 5% of chitin, and 57% of other polysaccharides (Pylkkänen et al., 2023).

International Journal of Current Science Research and Review
ISSN: 2581-8341
Volume 08 Issue 01 January 2025
DOI: 10.47191/ijcsrr/V8-i1-36, Impact Factor: 7.943
IJCSRR @ 2025
www.ijcsrr.org

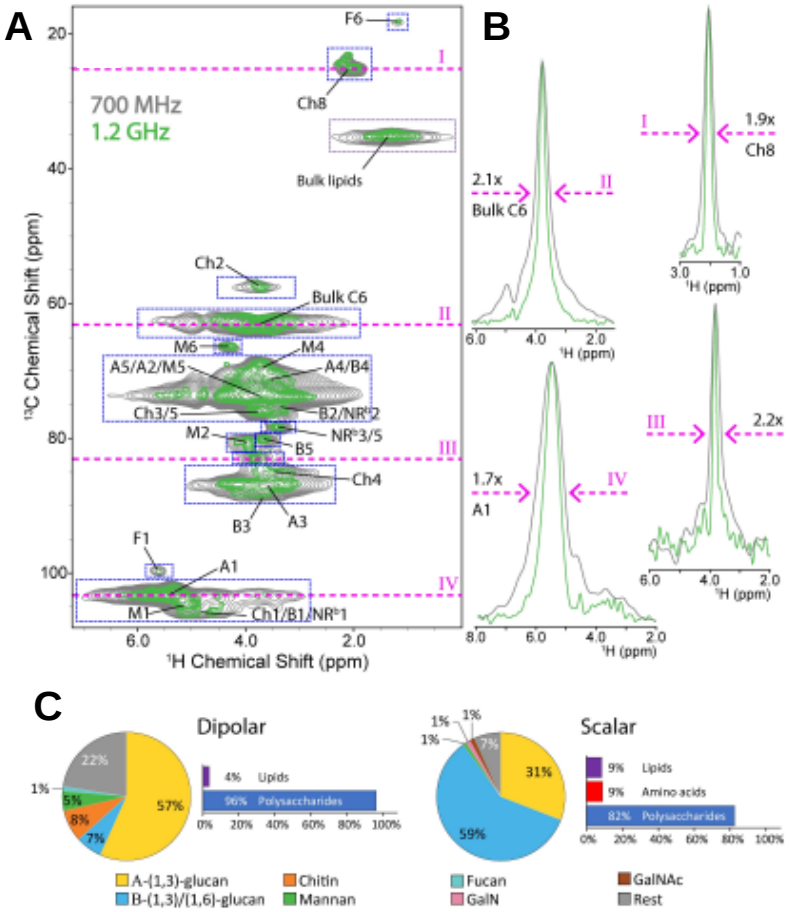

Figure 11. Peak linewidth improvement at 1.2 GHz vs. 700 MHz and the composition of the *S. commune* cell wall. **A.** An overlay of dipolar 2D CH-correlation spectra recorded at 1.2 GHz (green) and 700 MHz (grey), scaled to noise level. **B.** 1D slices (magenta lines) from the 2D spectra demonstrate improvement in peak linewidth at half height, scaled to maximum peak height. **C.** The relative abundance of rigid (dipolar) and flexible (scalar) cell wall polysaccharide species derived from 2D CH-correlation spectra. The employed integration areas for the quantification of rigid species are denoted by dashed boxes (blue) in A. This figure was reproduced from Safeer et al., 2023.

5. CONCLUSION

The development of ultra-high field NMR magnets (≥ 1 GHz) is one of the principal approaches contributing to an exciting period for improving the sensitivity and resolution in NMR spectroscopy. The demonstrated benefits of ultra-high field NMR for different applications, especially for challenging biological samples, have begun to emerge. With over twenty ultra-high field NMR instruments now installed worldwide, and with more to come, there should be a proliferation in analysing the structure, function and dynamics of biomolecules by NMR under conditions close to their native environment. Solution-state NMR enables the isolation and analysis of increasing numbers of conformational states of biomolecules and enables the dynamics of macromolecular complexes in solution to be studied that is difficult to achieve by X-ray crystallography or cryogenic electron microscopy. It also enables the analysis of whole cells, organelles and membraneless organelles. Solid-state NMR is unique for studying membrane proteins in their native membranes or in a lipid environment. For example, in analysing the structure and dynamics of drug binding to protein target sites such as GPCRs, to provide information for structure-based drug design. The unique capabilities of ultra-high field NMR will be especially powerful when combined with those of X-ray crystallography, cryogenic electron microscopy and other techniques in an integrated approach to structural biology, and drug design and discovery.

International Journal of Current Science Research and Review
ISSN: 2581-8341
Volume 08 Issue 01 January 2025
DOI: 10.47191/ijcsrr/V8-i1-36, Impact Factor: 7.943
IJCSRR @ 2025
www.ijcsrr.org

CONFLICT OF INTEREST

The author has no conflict of interest to declare.

REFERENCES

1. Ahmed, D., Cacciatore, S., and Zerbini, L. F. 2023. Metabolite analyses using nuclear magnetic resonance (NMR) spectroscopy in plasma of patients with prostate cancer. Methods Mol Biol 2675: 195-204.
2. Akutsu, H. 2023. Strategies for elucidation of the structure and function of the large membrane protein complex, FoF1-ATP synthase, by nuclear magnetic resonance. Biophys Chem 296: 106988.
3. Ardenkjaer-Larsen, J. H., Boebinger, G. S., Comment, A., Duckett, S., Edison, A. S., Engelke, F., Griesinger, C., Griffin, R. G., Hilty, C., Maeda, H., Parigi, G., Prisner, T., Ravera, E., van Bentum, J., Vega, S., Webb, A., Luchinat, C., Schwalbe, H., and Frydman, L. 2015. Facing and overcoming sensitivity challenges in biomolecular NMR spectroscopy. Angew Chem Int Ed Engl 54(32): 9162-9185.
4. Bahri, S., Safeer, A., Adler, A., Smedes, H., van Ingen, H., and Baldus, M. 2023. ^{1}H-detected characterization of carbon-carbon networks in highly flexible protonated biomolecules using MAS NMR. J Biomol NMR 77(3): 111-119.
5. Barnes, A. B., Paëpe, G. D., van der Wel, P. C., Hu, K. N., Joo, C. G., Bajaj, V. S., Mak-Jurkauskas, M. L., Sirigiri, J. R., Herzfeld, J., Temkin, R. J., and Griffin, R. G. 2008. High-field dynamic nuclear polarization for solid and solution biological NMR. Appl Magn Reson 34(3-4): 237-263.
6. Berge, A. H., Pugh, S. M., Short, M. I. M., Kaur, C., Lu, Z., Lee, J. H., Pickard, C. J., Sayari, A., and Forse, A. C. 2022. Revealing carbon capture chemistry with 17-oxygen NMR spectroscopy. Nat Commun 13(1): 7763.
7. Brown, S. P., and Su Y. 2023. Solid-state NMR of organic molecules: Characterising solid-state form. Solid State Nucl Magn Reson 126: 101876.
8. Caceres-Cortes, J., Falk, B., Mueller, L., and Dhar, T. G. M. 2024. Perspectives on nuclear magnetic resonance spectroscopy in drug discovery research. J Med Chem 67(3): 1701-1733.
9. Callon, M., Luder, D., Malär, A. A., Wiegand, T., Římal, V., Lecoq, L., Böckmann, A., Samoson, A., and Meier, B. H. 2023. High and fast: NMR protein-proton side-chain assignments at 160 kHz and 1.2 GHz. Chem Sci 14(39): 10824-10834.
10. Callon, M., Malär, A. A., Pfister, S., Římal, V., Weber, M. E., Wiegand, T., Zehnder, J., Chávez, M., Cadalbert, R., Deb, R., Däpp, A., Fogeron, M. L., Hunkeler, A., Lecoq, L., Torosyan, A., Zyla, D., Glockshuber, R., Jonas, S., Nassal, M., Ernst, M., Böckmann, A., and Meier, B. H. 2021. Biomolecular solid-state NMR spectroscopy at 1200 MHz: The gain in resolution. J Biomol NMR 75(6-7): 255-272.
11. Camacho-Zarco, A. R., Schnapka, V., Guseva, S., Abyzov, A., Adamski, W., Milles, S., Jensen, M. R., Zidek, L., Salvi, N., and Blackledge, M. 2022. NMR provides unique insight into the functional dynamics and interactions of intrinsically disordered proteins. Chem Rev 122(10): 9331-9356.
12. Cao, R., Liu, X., Liu, Y., Zhai, X., Cao, T., Wang, A., and Qiu, J. 2021. Applications of nuclear magnetic resonance spectroscopy to the evaluation of complex food constituents. Food Chem 342: 128258.
13. Derome, E. 1987. Modern NMR techniques for chemistry research. Elsevier Science Ltd, London.
14. Dinclaux, M., Cahoreau, E., Millard, P., Létisse, F., and Lippens, G. 2020. Increasing field strength versus advanced isotope labeling for NMR-based fluxomics. Magn Reson Chem 58(4): 305-311.
15. Dsouza, L., Li, X., Erić, V., Huijser, A., Jansen, T. L. C., Holzwarth, A. R., Buda, F., Bryant, D. A., Bahri, S., Gupta, K. B. S. S, Sevink, G. J. A., and de Groot, H. J. M. 2024. An integrated approach towards extracting structural characteristics of chlorosomes from a bchQ mutant of *Chlorobaculum tepidum*. Phys Chem Chem Phys 26(22): 15856-15867.
16. Du, M. 2023. Approaches to NMR sensitivity enhancement based on theoretical analysis. J Phys: Conf Ser 2634: 012023.
17. Dyson, H. J., and Wright, P. E. 2019. Perspective: The essential role of NMR in the discovery and characterization of intrinsically disordered proteins. J Biomol NMR 73(12): 651-659.
18. El Sabbagh, N., Bonny, J. M., Clerjon, S., Chassain, C., and Pagés, G. 2022. Characterization of the sodium binding state in several food products by ^{23}Na nuclear magnetic resonance spectroscopy. Magn Reson Chem 60(7): 597-605.
19. Emwas, A.-H., Roy, R., McKay, R. T., Tenori, L., Saccenti, E., Gowda, G. A. N., Raftery, D., Alahmari, F., Jaremko, L., Jaremko, M., and Wishart, D. S. 2019. NMR spectroscopy for metabolomics research. Metabolites 9(7): 123.

International Journal of Current Science Research and Review
ISSN: 2581-8341
Volume 08 Issue 01 January 2025
DOI: 10.47191/ijcsrr/V8-i1-36, Impact Factor: 7.943
IJCSRR @ 2025
www.ijcsrr.org

20. Emwas A.-H., Szczepski, K., Poulson, B. G., Chandra, K., McKay, R. T., Dhahri, M., Alahmari, F., Jaremko, L., Lachowicz, J.I., and Jaremko, M. 2020. NMR as a "gold standard" method in drug design and discovery. Molecules 25(20): 4597.
21. Farrar, C. T., Hall, D. A., Gerfen, G. J., Rosay, M., Ardenkjaer-Larsen, J. H., and Griffin, R. G. 2000. High-frequency dynamic nuclear polarization in the nuclear rotating frame. J Magn Reson 144(1): 134-141.
22. Florea, I., Jumate, E., Manea, D. L., and Fechete, R. 2019. NMR study on new natural building materials. Procedia Manufacturing 32: 224-229.
23. Gan, Z., Hung, I., Wang, X., Paulino, J., Wu, G., Litvak, I. M., Gor'kov, P. L., Brey, W. W., Lendi, P., Schiano, J. L., Bird, M. D., Dixon, I. R., Toth, J., Boebinger, G. S., and Cross, T. A. 2017. NMR spectroscopy up to 35.2T using a series-connected hybrid magnet. J Magn Reson 284: 125-136.
24. Gerez, J. A., Prymaczok, N. C., Kadavath, H., Ghosh, D., Bütikofer, M., Fleischmann, Y., Güntert, P., and Riek, R. 2022. Protein structure determination in human cells by in-cell NMR and a reporter system to optimize protein delivery or transexpression. Commun Biol 5(1): 1322.
25. Grover, V. P., Tognarelli, J. M., Crossey, M. M., Cox, I. J., Taylor-Robinson, S. D, and McPhail, M. J. 2015. Magnetic resonance imaging: Principles and techniques: Lessons for clinicians. J Clin Exp Hepatol 5(3): 246-255.
26. Hiruma-Shimizu, K., Shimizu, H., Thompson, G. S., Kalverda, A. P., and Patching, S. G. 2015. Deuterated detergents for structural and functional studies of membrane proteins: Properties, chemical synthesis and applications. Mol Membr Biol 32(5-8): 139-155.
27. Horrocks, V., Hind, C. K., Wand, M. E., Fady, P. E., Chan, J., Hopkins, J. C., Houston, G. L., Tribe, R. M., Sutton, J. M., and Mason, A. J. 2022. Nuclear magnetic resonance metabolomics of symbioses between bacterial vaginosis-associated bacteria. mSphere 7(3): e0016622.
28. Hu, J., Kim, J., and Hilty, C. 2022. Detection of protein-ligand interactions by ^{19}F nuclear magnetic resonance using hyperpolarized water. J Phys Chem Lett 13(17): 3819-3823.
29. Kadavath, H., Cecilia Prymaczok, N., Eichmann, C., Riek, R., and Gerez, J. A. 2023. Multi-dimensional structure and dynamics landscape of proteins in mammalian cells revealed by in-cell NMR. Angew Chem Int Ed Engl 62(4): e202213976.
30. Kalverda, A. P., Gowdy, J., Thompson, G. S., Homans, S. W., Henderson, P. J., and Patching, S. G. 2014. TROSY NMR with a 52 kDa sugar transport protein and the binding of a small-molecule inhibitor. Mol Membr Biol 31(4): 131-140.
31. Kaup, R., and Velders, A. H. 2022. Controlling trapping, release, and exchange dynamics of micellar core components. ACS Nano 16(9): 14611-14621.
32. Keeler, J. 2010. Understanding NMR spectroscopy. Wiley.
33. Khasham,i F. 2024. Fundamentals of NMR and MRI: From quantum principles to medical applications. Springer Cham.
34. Kruschwitz, S., Munsch, S., Telong, M., Schmidt, W., Bintz, T., Fladt, M., and Stelzner, M. 2023. The NMR core analyzing tomograph: A multi-functional tool for non-destructive testing of building materials. Magn Reson Lett 3(3): 207-219.
35. Lacey, M. E., Subramanian, R., Olson, D. L., Webb, A. G., and Sweedler, J. V. 1999. High-resolution NMR spectroscopy of sample volumes from 1 nL to 10 µL. Chem Rev 99(10): 3133-3152.
36. Leifer, N., Aurbach, D., and Greenbaum, S. G. 2024. NMR studies of lithium and sodium battery electrolytes. Prog Nucl Magn Reson Spectrosc 142-143: 1-54.
37. Levitt, M. H. 2001. Spin dynamics: Basics of nuclear magnetic resonance. Wiley-Blackwell.
38. Luchinat, E., and Banci, L. 2022. In-cell NMR: From target structure and dynamics to drug screening. Curr Opin Struct Biol 74: 102374.
39. Luchinat, E., Barbieri, L., Cremonini, M., and Banci, L. 2021b. Protein in-cell NMR spectroscopy at 1.2 GHz. J Biomol NMR 75(2-3): 97-107.
40. Luchinat, E., Barbieri, L., Cremonini, M., Pennestri, M., Nocentini, A., Supuran, C. T., and Banci, L. 2021a. Determination of intracellular protein-ligand binding affinity by competition binding in-cell NMR. Acta Crystallogr D Struct Biol 77(Pt 10): 1270-1281.
41. Marchand, J., Martineau, E., Guitton, Y., Dervilly-Pinel, G., and Giraudeau, P. 2017. Multidimensional NMR approaches towards highly resolved, sensitive and high-throughput quantitative metabolomics. Curr Opin Biotechnol 43: 49-55.

International Journal of Current Science Research and Review
ISSN: 2581-8341
Volume 08 Issue 01 January 2025
DOI: 10.47191/ijcsrr/V8-i1-36, Impact Factor: 7.943
IJCSRR @ 2025
www.ijcsrr.org

42. Mauri, M., and Simonutti, R. 2012. Hyperpolarized xenon nuclear magnetic resonance (NMR) of building stone materials. Materials 5(9): 1722-1739.
43. Moser, E., Laistler, E., Schmitt, F., and Kontaxis, G. 2017. Ultra-high field NMR and MRI-the role of magnet technology to increase sensitivity and specificity. Front Phys 5(33): 1-15.
44. Nagana Gowda, G. A., and Raftery, D. 2023. NMR metabolomics methods for investigating disease. Anal Chem 95(1): 83-99.
45. Nawaz, N., and Patching, S. G. 2023. Polarising agents and spin tags for dynamic nuclear polarisation (DNP)-enhanced solid-state nuclear magnetic resonance (ssNMR) analysis of biological samples. Curr J Appl Sci Technol 42(28): 11-38.
46. Nimerovsky, E., Movellan, K. T., Zhang, X. C., Forster, M. C., Najbauer, E., Xue, K., Dervişoğlu, R., Giller, K., Griesinger, C., Becker, S., and Andreas, L. B. 2021. Proton detected solid-state NMR of membrane proteins at 28 Tesla (1.2 GHz) and 100 kHz magic-angle spinning. Biomolecules 11(5): 752.
47. Oliveira, D. R., da Costa, E. T., Schenberg, L. A., Ducati, L. C., and do Lago, C. L. 2024. ^{13}C NMR as an analytical tool for the detection of carbonic acid and pKa determination. Magn Reson Chem 62(2): 114-120.
48. Park, D., Lee, J., Bascuñán, J., Li, Z., and Iwasa, Y. 2020. Prototype REBCO Z1 and Z2 shim coils for ultra high-field. Sci Rep 10(1): 21946.
49. Patching, S. G. 2011. NMR structures of polytopic integral membrane proteins. Mol Membr Biol 28(6): 370-397.
50. Patching, S. G. 2015. Solid-state NMR structures of integral membrane proteins. Mol Membr Biol 32(5-8): 156-178.
51. Patching, S. G. 2016. NMR-active nuclei for biological and biomedical applications. Journal of Diagnostic Imaging in Therapy 3(1): 7-48.
52. Patching, S. G. 2017. Synthesis, NMR analysis and applications of isotope-labelled hydantoins. J Diagn Imag Ther 4(1): 3-26.
53. Patching, S. G, Edwards, R., and Middleton, D. A. 2009. Structural analysis of uniformly ^{13}C-labelled solids from selective angle measurements at rotational resonance. J Magn Reson 199(2): 242-246.
54. Plavec, J. 2022. NMR study on nucleic acids. In: Sugimoto N (Ed) Handbook of Chemical Biology of Nucleic Acids. Springer, Singapore. DOI: 10.1007/978-981-16-1313-5_8-1
55. Pugh, S. M., and Forse, A. C. 2023. Nuclear magnetic resonance studies of carbon dioxide capture. J Magn Reson 346: 107343.
56. Pylkkänen, R., Werner, D., Bishoyi, A., Weil, D., Scoppola, E., Wagermaier, W., Safeer, A., Bahri, S., Baldus, M., Paananen, A., Penttilä, M., Szilvay, G. R., and Mohammadi, P. 2023. The complex structure of *Fomes fomentarius* represents an architectural design for high-performance ultralightweight materials. Sci Adv 9(8): eade5417.
57. Quinn, C. M., Zadorozhnyi, R., Struppe, J., Sergeyev, I. V., Gronenborn, A. M., and Polenova, T. 2021. Fast ^{19}F magic-angle spinning nuclear magnetic resonance for the structural characterization of active pharmaceutical ingredients in blockbuster drugs. Anal Chem 93(38): 13029-13037.
58. Razew, A., Herail, Q., Miyachiro, M., Anoyatis-Pelé, C., Bougault, C., Dessen, A., Arthur, M., and Simorre, J. P. 2014. Monitoring drug-protein interactions in the bacterial periplasm by solution nuclear magnetic resonance spectroscopy. J Am Chem Soc 146(13): 9252-9260.
59. Richards, S. A., and Hollerton, J. C. 2010. Essential practical NMR for organic chemistry. Wiley.
60. Safeer, A., Kleijburg, F., Bahri, S., Beriashvili, D., Veldhuizen, E. J. A., van Neer, J., Tegelaar, M., de Cock, H., Wösten, H. A. B, and Baldus, M. 2023. Probing cell-surface interactions in fungal cell walls by high-resolution ^{1}H-detected solid-state NMR spectroscopy. Chemistry 29(1): e202202616.
61. Saurel, O., Iordanov, I., Nars, G., Demange, P., Le Marchand, T., Andreas, L. B., Pintacuda, G., and Milon, A. 2017. Local and global dynamics in *Klebsiella pneumoniae* outer membrane protein A in lipid bilayers probed at atomic resolution. J Am Chem Soc 139(4): 1590-1597.
62. Schiavina, M., Bracaglia, L., Rodella, M. A., Kümmerle, R., Konrat, R., Felli, I. C., and Pierattelli, R. 2024. Optimal ^{13}C NMR investigation of intrinsically disordered proteins at 1.2 GHz. Nat Protoc 19(2): 406-440.
63. Schiavina, M., Murrali, M. G., Pontoriero, L., Sainati, V., Kümmerle, R., Bermel, W., Pierattelli, R., and Felli, I. C. 2019. Taking simultaneous snapshots of intrinsically disordered proteins in action. Biophys J 117(1): 46-55.

64. Schiavina, M., Pontoriero, L., Tagliaferro, G., Pierattelli, R., and Felli, I. C. 2022. The role of disordered regions in orchestrating the properties of multidomain proteins: The SARS-CoV-2 nucleocapsid protein and its interaction with enoxaparin. Biomolecules 12(9): 1302.
65. Schubeis, T., Schwarzer, T. S., Le Marchand, T., Stanek, J., Movellan, K. T., Castiglione, K., Pintacuda, G., and 2020. Andreas, L. B. Resonance assignment of the outer membrane protein AlkL in lipid bilayers by proton-detected solid-state NMR. Biomol NMR Assign 14(2): 295-300.
66. Shahrajabian, M. H., and Sun, W. 2024. Characterization of intrinsically disordered proteins in healthy and diseased states by nuclear magnetic resonance. Rev Recent Clin Trials 19(3): 176-188.
67. Shan, P., Chen, J., Tao, M., Zhao, D., Lin, H., Fu, R., and Yang, Y. 2023. The applications of solid-state NMR and MRI techniques in the study of rechargeable sodium-ion batteries. J Magn Reson 353: 107516.
68. Tsiafoulis, C. G., Liaggou, C., Garoufis, A., Magiatis, P., and Roussis, I. G. 2024. Nuclear magnetic resonance analysis of extra virgin olive oil: Classification through secoiridoids. J Sci Food Agric 104(4): 1992-2005.
69. Walder, B. J., Conradi, M. S., Borchardt, J. J., Merrill, L. C., Sorte, E. G., Deichmann, E. J., Anderson, T. M., Alam, T. M., and Harrison, K. L. 2021. NMR spectroscopy of coin cell batteries with metal casings. Sci Adv 7(37): eabg8298.
70. Wang, X., Akhmedov, N. G., Duan, Y., and Li, B. 2015. Nuclear magnetic resonance studies of CO_2 absorption and desorption in aqueous sodium salt of alanine. Energy and Fuels 29(6): 3780-3784.
71. Webb, A. 2012. Increasing the sensitivity of magnetic resonance spectroscopy and imaging. Anal Chem 84(1): 9-16.
72. Weng, J., Muti, I. H., Zhong, A. B., Kivisäkk, P., Hyman, B. T., Arnold, S. E., and Cheng, L. L. 2022. A nuclear magnetic resonance spectroscopy method in characterization of blood metabolomics for Alzheimer's disease. Metabolites 12(2): 181.
73. Wikus, P., Frantz, W., Kümmerle, R., and Vonlanthen, P. 2022. Commercial gigahertz-class NMR magnets. Supercond Sci Technol 35(3): 033001.
74. Xue, K., Sarkar, R., Tosner, Z., Lalli, D., Motz, C., Koch, B., Pintacuda, G., and Reif, B. 2019. MAS dependent sensitivity of different isotopomers in selectively methyl protonated protein samples in solid state NMR. J Biomol NMR 73(10-11): 625-631.
75. Yamaoki, Y., Nagata, T., Sakamoto, T., and Katahira, M. 2020. Recent progress of in-cell NMR of nucleic acids in living human cells. Biophys Rev 12(2): 411-417.
76. Zheng, A., and Greenbaum, S. G. 2023. NMR studies of polymeric sodium ion conductors-a brief review. Front Chem 11: 1296587.